

TWO REGIMES OF TURBULENT FRAGMENTATION AND THE STELLAR IMF FROM PRIMORDIAL TO PRESENT DAY STAR FORMATION

PAOLO PADOAN¹, ÅKE NORDLUND², ALEXEI G. KRITSUK¹, MICHAEL L. NORMAN¹, PAK SHING LI

Draft version May 26, 2019

ABSTRACT

The Padoan and Nordlund model of the stellar initial mass function (IMF) is derived from low order statistics of supersonic turbulence, neglecting gravity (e.g. gravitational fragmentation, accretion and merging). In this work the predictions of that model are tested using the largest numerical experiments of supersonic hydrodynamic (HD) and magneto-hydrodynamic (MHD) turbulence to date ($\sim 1000^3$ computational zones) and three different codes (Enzo, Zeus and the Stagger Code). The model predicts a power law distribution for large masses, related to the turbulence energy power spectrum slope, and the shock jump conditions. This power law mass distribution is confirmed by the numerical experiments. The model also predicts a sharp difference between the HD and MHD regimes, which is recovered in the experiments as well, implying that the magnetic field, even below energy equipartition on the large scale, is a crucial component of the process of turbulent fragmentation. These results suggest that the stellar IMF of primordial stars may differ from that in later epochs of star formation, due to differences in both gas temperature and magnetic field strength. In particular, we find that the IMF of primordial stars born in turbulent clouds may be narrowly peaked around a mass of order $10 M_{\odot}$, as long as the column density of such clouds is not much in excess of 10^{22} cm^{-2} .

Subject headings: ISM: kinematics and dynamics — stars: formation — turbulence

1. INTRODUCTION

In the turbulent fragmentation model of Padoan & Nordlund (2002), the mass distribution of gravitationally unstable cores in turbulent clouds is derived from low order statistics of supersonic turbulence (the one-point pdf of gas density, and the first-order scaling of velocity differences -though we refer to the velocity power spectrum, as a second order proxy of the first order scaling) and from focusing on the fundamental flow geometry of shock compressions. This is a natural (if not traditional) approach to the solution of a very complex turbulence problem, because a simple solution must be based on low order statistics giving the basic variance and scaling of the process. But low order statistics cannot capture the flow geometry. Instead of relying on closure models of a statistical nature, an alternative is to impose some knowledge of a fundamental flow feature that would otherwise be hard to capture with statistical quantities. This is especially true because of the strong intermittent nature of turbulent flows, meaning that the most important flow structures could be properly accounted for only by very high order statistics, so relatively low order statistical closure models are bound to largely overlook those important structures. A phenomenological model centered on the geometry of those structures, in combination with low order statistics is therefore a valid alternative, and it is the approach of choice in the work of Padoan & Nordlund (2002).

The model assumes that: i) the turbulence has a power law velocity power spectrum (the model really uses the

first order scaling of velocity differences, but that is related to the power spectrum anyway); ii) cores are formed by shocks in the turbulent flow and have size and density that scale as the postshock layer thickness and density; iii) the number of such shocks scales self-similarly as the inverse of the cube of their size; iv) the condition for the collapse of small cores is that their mass exceeds their Bonnor-Ebert mass, derived from the lognormal probability density function (pdf) of the gas density independently of the core mass.

These assumptions are all reasonable for an approximately isothermal and supersonic turbulent gas. The first assumption is a well established result for turbulent flows. The second assumption is suggested by the simulations, where the unstable cores are always found to be the densest regions of postshock sheets or filaments. The third assumption is motivated by the very large Reynolds number of the turbulence in star-forming clouds, which is expected to generate a very extended inertial range of scales and possibly a self-similar flow responsible for the network of shocks (this self-similarity does not imply necessarily a hierarchical, space-filling nested structure, where smaller compressing regions would always be inside larger ones). Finally, the fourth assumption stems from the fact that most of the densest gas is located within dense cores, so the high density tail of the gas density pdf should be well represented by the distribution of the core mean density.

These assumptions result in a power law mass distribution reflecting the scale-free nature of the turbulence, and a turnover at small masses, where gas pressure competes with self-gravity. After integrating over the probability of exceeding the Bonnor-Ebert mass, the mass distribution is given by the following formula:

$$N(m)dm = C \left[1 + \operatorname{erf} \left(\frac{4\ln(m) + \sigma^2}{2\sqrt{2}\sigma} \right) \right] m^{-x} dm \quad (1)$$

¹ Department of Physics, University of California, San Diego, CASS/UCSD 0424, 9500 Gilman Drive, La Jolla, CA 92093-0424; ppadoan@ucsd.edu

² Astronomical Observatory / NBIfAFG, Juliane Maries Vej 30, DK-2100, Copenhagen, Denmark

³ Astronomy Department, University of California, Berkeley, CA 94720

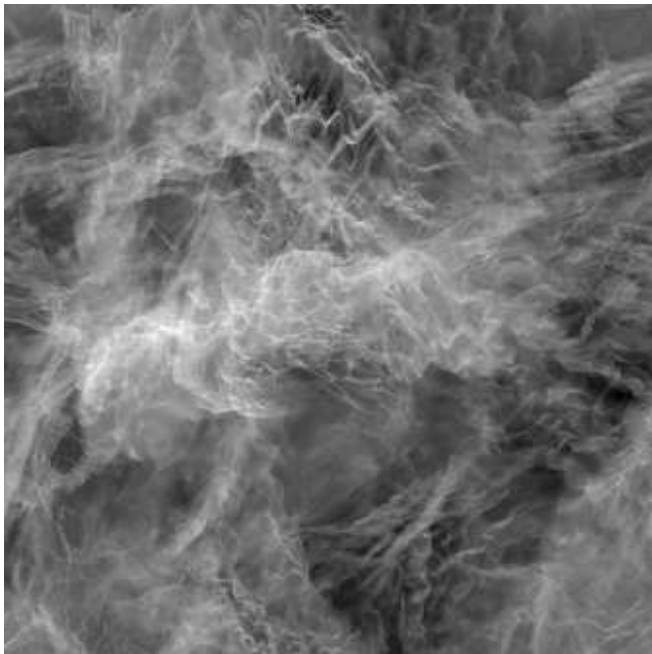


FIG. 1.— Logarithm of projected density from a snapshot of the Stagger-Code HD run.

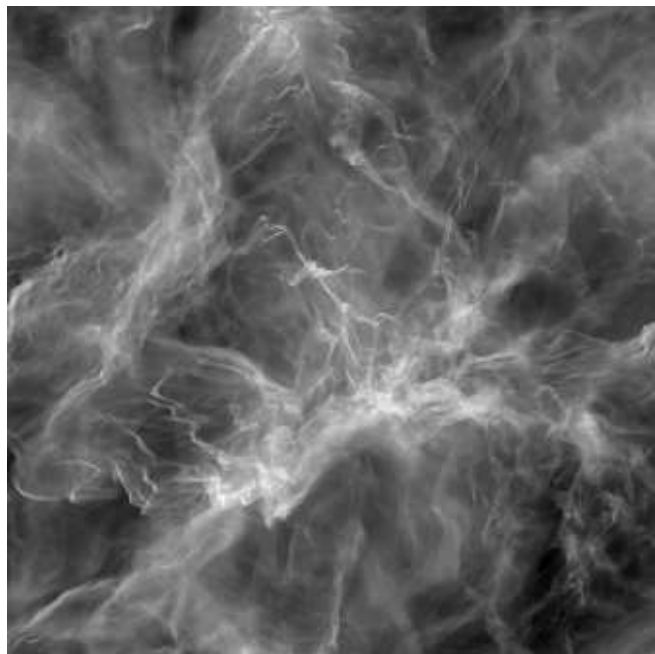


FIG. 2.— Logarithm of projected density from a snapshot of the Stagger-Code MHD run.

where the mass m is in units of the average Bonnor-Ebert mass,

$$m_{\text{BE},o} = 3.3M_{\odot} \left(\frac{n_o}{10^3 \text{cm}^{-3}} \right)^{-1/2} \left(\frac{T_o}{10\text{K}} \right)^{3/2}, \quad (2)$$

σ is the standard deviation of the gas density pdf (assumed to be a lognormal) related to the rms Mach number of the turbulence (the sonic or the Alfvénic Mach number in the HD or MHD regime respectively, see below):

$$\sigma = \sqrt{\ln(1 + M_o^2/4)} \quad (3)$$

(from here on the subscript o denotes quantities averaged on the outer scale of the turbulence). The coefficient C depends on the physical parameters and is not discussed here because the normalization of the mass distribution is not required for this work. The power law slope, x , is determined by the power law slope of the energy spectrum, β ($\beta \approx 5/3$ in incompressible turbulence and $\beta = 2$ in Burgers zero-pressure model), and by the shock jump conditions:

$$x = 3/(4 - \beta) \quad (4)$$

for $B \geq B_{\text{cr}}$ (MHD jump conditions), and

$$x = 3/(5 - 2\beta) \quad (5)$$

for $B < B_{\text{cr}}$ (isothermal HD jump conditions). The critical magnetic field value that separates the two regimes is given by the condition that the postshock gas pressure is of order the postshock magnetic pressure, corresponding to an rms Alfvénic Mach number, M_A , of the order of the ratio of the mean gas and magnetic pressures, $M_A \sim P_g/P_m$. This condition gives

$$B_{\text{cr}} \approx 2\mu\text{G} \left(\frac{T_o}{10\text{K}} \right) \left(\frac{u_o}{1\text{km/s}} \right)^{-1} \left(\frac{n_o}{10^3 \text{cm}^{-3}} \right)^{1/2} \quad (6)$$

Because the Galactic magnetic field strength is locally

$6 \pm 2 \mu\text{G}$ (Beck 2001; Han, Ferrière, & Manchester 2004), and perhaps larger in molecular cloud cores (Crutcher 1999; Bourke et al. 2001), current star formation in the galactic disk occurs under MHD conditions. For a value of $\beta = 1.9$, found from the least dissipative simulations in this work, the predicted slope of the mass distribution of prestellar cores is then $x = 1.4$, practically the same as the Salpeter slope of the stellar IMF ($x = 1.35$, Salpeter 1955). For very weak magnetic fields, perhaps in protogalaxies at very large redshifts, the slope would be $x = 2.5$, assuming again $\beta = 1.9$. Furthermore, conditions at high redshifts and very low or zero metallicity would also include a larger temperature, $T > 100\text{K}$ (e.g. Palla, Salpeter, & Stahler 1983; Abel, Bryan & Norman 2000). The larger temperature results in a value of B_{cr} at least 10 times larger than in present day environments with the same rms velocity and mean density, making the HD regime, and hence the steeper IMF, even more likely to occur for stellar populations at high redshift. At the same time, the larger temperature also shifts the peak of the IMF to larger masses, according to equations (1) and (2). Although the first population III stars are usually believed to form in isolation in the cores of very small halos, population III stars formed somewhat later and in somewhat more massive halos (Jimenez & Haiman 2006; Iliev et al. 2006) may indeed emerge from turbulent star-forming environments more akin to current star formation sites. Thus, the steeper IMF for massive stars corresponding to the HD regime may also apply to bona-fide population III stars, as well as to early population II stars.

The peak of the distribution shifts to smaller masses with increasing Mach number and gas density, which also increases the abundance of low mass stars and brown dwarfs. For reasonable values of the physical parameters, this mass distribution becomes essentially the same

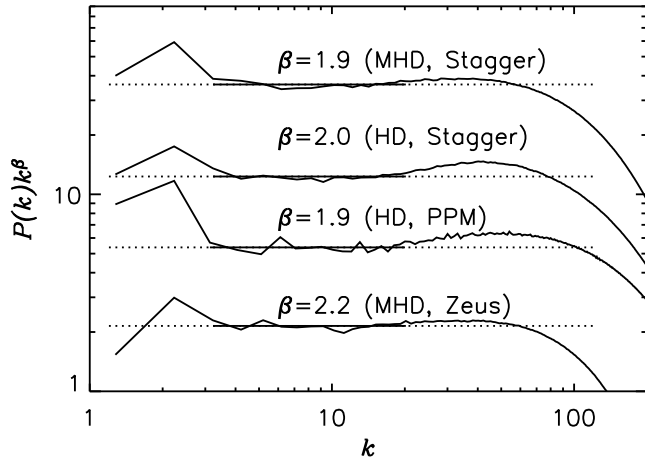


FIG. 3.— Compensated power spectra of the main four runs and least square fits in the range of wavenumbers $3 \leq k \leq 20$.

as the observed stellar IMF in Chabrier (2003). This coincidence suggests that the process of turbulent fragmentation may play a major role in the origin of the stellar IMF (Padoan & Nordlund 2002), with only minor effects due to gravitational fragmentation, accretion or merging.

A numerical estimate of the dependence of the peak mass on the rms Mach number gives:

$$m_p = 3.0 M_0^{-1.1} M_{BE,0} \quad (7)$$

assuming $x = 1.4$ (MHD regime), and

$$m_p = 3.9 M_0^{-1.7} M_{BE,0} \quad (8)$$

assuming $x = 2.5$ (HD regime). In the following we relate m_p to the peak of the stellar IMF. Since the latter can be accurately determined observationally only for stellar clusters, presumably formed in gravitationally bound cores, we may assume the gas velocity dispersion is of order the virial velocity. With this assumption, and using the rms Alfvénic Mach number, equation (7) gives:

$$m_p = 0.25 M_\odot N_{0,22}^{-1.1} B_{0,10}^{1.1} n_{0,4}^{-1/2} T_{0,10}^{3/2} \quad (9)$$

where $N_{0,22}$, $B_{0,10}$, $n_{0,4}$, and $T_{0,10}$ are the mean column density, magnetic field, particle density and temperature in units of 10^{22} cm^{-2} , $10 \mu\text{G}$, 10^4 cm^{-3} , and 10 K respectively, which are typical values for star-forming cloud cores. This value of m_p provides an estimate of the peak of the stellar IMF (although it should be somewhat larger than the IMF peak because a fraction of the core mass is not accreted onto the star and because some cores may result in binaries or multiple systems).

The observed IMF (of multiple systems) peaks at roughly $0.2 M_\odot$ (Chabrier 2003), with no clear evidence of a strong departure from this value in any star-forming region, with the exception of the Taurus molecular cloud complex (Luhman 2004). As both temperature and column density don't have very large variations from cloud to cloud, our fragmentation model would predict a nearly constant value of m_p if $B_0 \propto n_0^{0.45}$, for which there is some observational and theoretical support (Myers & Goodman 1988; Crutcher 1999; Padoan & Nordlund 1999; Basu 2000). Sites of massive star formation may have larger mean column density, but they also have

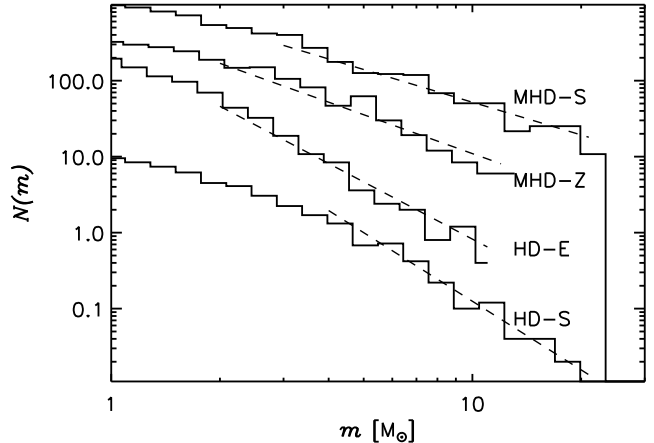


FIG. 4.— Mass distributions of gravitationally unstable cores above $1 M_\odot$, for the main four experiments scaled to a mean density of 10^4 cm^{-3} , a box size of 6 pc, and a clumpfind density resolution $f = 8\%$. The dashed lines show the power law derived from the power spectrum slope and the shock jump conditions of the corresponding simulations, according to the turbulent fragmentation model. The histograms are arbitrarily offset in the vertical direction for clarity.

larger temperature than regions of low-mass star formation (e.g. Ossenkopf, Trojan, & Stutzki 2001; Beuther et al. 2006), which may result in a similar value of m_p .

In the HD regime, assuming again virial velocity dispersion and using the sonic rms Mach number, the peak mass given by equation (8) is:

$$m_p = 0.16 M_\odot N_{0,22}^{-1.7} n_{0,4}^{0.35} T_{0,10}^{3/2} \quad (10)$$

Because this regime may be relevant for very low to zero metallicity, the temperature may exceed 200 K, resulting in a value of $m_p > 14 M_\odot$. It has been often proposed that the IMF of population III stars should contain an excess of massive stars relative to the present day IMF. This may indeed occur with our IMF in the HD regime, despite its steep slope, due the high gas temperature of primordial gas, shifting the peak of the IMF toward large masses. Because of its steep slope, though, *the IMF of primordial stars would then be narrowly peaked around a large mass of order $10 M_\odot$* . On the other hand, even if $T_0 = 200 \text{ K}$, a very large column density of order $N_0 = 10^{23} \text{ cm}^{-2}$, would give $m_p = 0.3 M_\odot$, similar to the IMF peak in regions of present-day star formation. This example shows that the typical mass of primordial stars born in turbulent clouds cannot be estimated without a reliable value of the average column density of such clouds.

2. THE SIMULATIONS

As the turbulent fragmentation model outlined in the previous section neglects gravity (apart from the selection of unstable cores), its predictions can be tested with numerical simulations of supersonic MHD turbulence. However, because the model relies on the scale-free nature of the turbulence, it cannot be easily tested unless an extended inertial range of the turbulence is generated in the simulations, which requires both large numerical resolution (large computers) and low numerical diffusivity (good codes). The main comparison between the MHD

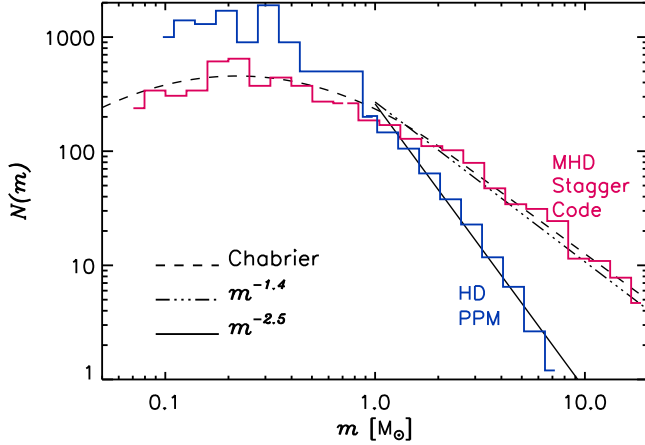


FIG. 5.— Mass distributions of gravitationally unstable cores from the HD and MHD regimes (Enzo and Stagger Code respectively), computed with $f = 16\%$ and assuming a mean gas density of 10^4 cm^{-3} . Each mass distribution is the result of matching two mass distributions, computed for a computational box size of 1 pc and 6 pc. The Chabrier IMF (Chabrier 2003) and the fragmentation model predictions for the power law mass distributions of each run are also plotted.

and HD regimes is here based on simulations with the Stagger Code, on a numerical mesh of $1,000^3$ computational zones. In order to rule out numerical artifacts of a specific code, we also simulated the HD regime with the Enzo code (Norman & Bryan 1999), and the MHD regime with the Zeus code (Stone & Norman 1992), in both cases on a numerical mesh of $1,024^3$ computational zones. The three codes are quite different from each other. Enzo is based on a Riemann solver and PPM reconstruction, the Stagger code is based on a high order (5th order in space, 4th order in time) finite difference scheme, and Zeus is a low order (2nd order in space, 1st order in time) finite difference code.

All simulations make use of periodic boundary conditions, isothermal equation of state, random forcing in Fourier space at wavenumbers $1 \leq k \leq 2$ ($k = 1$ correspond to the computational box size), uniform initial density and magnetic field (in the MHD runs), random initial velocity field with power only at wavenumbers $1 \leq k \leq 2$. The simulations are run for several dynamical times to relax the turbulence at rms Mach numbers of 6 or 10, before being analyzed. All results in this paper are for rms Mach number 10, unless otherwise specified. In Figures 1 and 2 we show two projections of the density field, from the HD and MHD Stagger Code runs. The density field in the HD run appears to be significantly more fragmented than its MHD counterpart. There are two main reasons for this difference: i) The density contrast in the HD shocks is larger than in the MHD shocks, creating thinner postshock layers from shocks with equal sonic Mach number; ii) the HD postshock layers are Kelvin-Helmholtz unstable, due to the strong shear flow that originates in oblique shocks, while in most of the MHD layers the same instability is suppressed by the magnetic field that is amplified in the compression. The turbulent fragmentation model of Padoan and Nordlund (2002) makes explicit use of the shock jump conditions, which results in the prediction

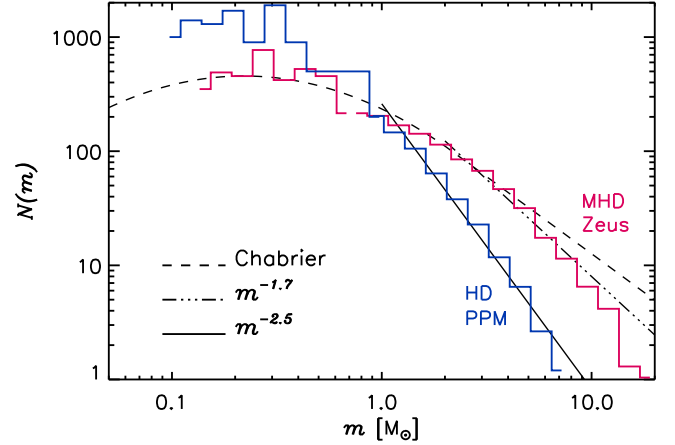


FIG. 6.— Same as Figure 5, but for the Zeus MHD run instead of the Stagger-Code MHD run. Notice how the steeper Zeus mass distribution is recovered. The model predicts the Zeus mass distribution to be steeper than the Stagger-Code one, as a result of the steeper turbulence power spectrum in the more diffusive Zeus run.

of a steeper mass distribution in the power law range of masses in the HD case than in the MHD one, but no direct reference to instabilities in the layers.

Figure 3 shows the compensated power spectra of the four main simulations. The power spectra are defined as the squared of the modulus of the Fourier transform of the velocity, integrated over a wave-number shell. If $\hat{\mathbf{u}}_i(\mathbf{k})$ is the Fourier transform of the i velocity component, $\mathbf{u}_i(\mathbf{r})$, the power spectrum is $P_i(k) = \sum \hat{\mathbf{u}}_i \hat{\mathbf{u}}_i^*$, where the sum is over all i and all wave-numbers \mathbf{k} in the shell $k \leq |\mathbf{k}| < k + dk$. $P(k)$ is proportional to the contribution to the mean square velocity from all wave-numbers in the shell $k \leq |\mathbf{k}| < k + dk$.

The plots in Figure 3 have been arbitrarily shifted in the vertical direction. Deviations of more than a factor of two from a power law fit are found only at wavenumbers $k > 100$, so the turbulence is roughly scale-free for almost two orders of magnitude in wavenumbers. The power law slopes depend somewhat on the exact range of wavenumbers used in the fit. We have chosen to measure the power spectrum slope in the range $3 \leq k \leq 20$, because larger wavenumbers are affected by the bottleneck effect (e.g. Falkovich 1994; Dobler et al. 2003; Haugen & Brandenburg 2004). If the least square fits were extended up to $k = 100$, to estimate an effective power spectrum slope relevant for the turbulent fragmentation process, the slopes would be only slightly different. We get $\beta = 1.9$ and 2.0 from the Stagger code in the MHD and HD regimes respectively. The Enzo code in the HD regime gives $\beta = 1.9$, and Zeus in the MHD regime $\beta = 2.2$. The corresponding values of the exponent of the power law range of the mass distribution of unstable cores are, according to the model of turbulent fragmentation, $x = 1.4$ and 3 for the MHD and HD regimes of the Stagger code, and $x = 1.7$ and 2.5 for the MHD and HD regimes of Zeus and Enzo respectively.

The power spectra show that the Stagger code is only slightly more dissipative than Enzo, while Zeus is significantly more dissipative than both. The numerical dissipation results in a power spectrum that is well fit by an extended power law, partly because an effect of

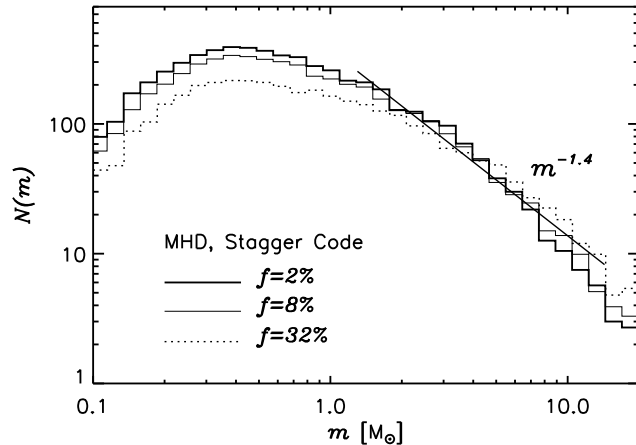


FIG. 7.— Test of convergence of the mass distribution with decreasing value of the density resolution parameter, f , from the Stagger-Code MHD run. The mass distribution is well converged at $f = 8\%$.

the numerical dissipation is to suppress the bump of excess power corresponding to the bottleneck effect, visible especially in the least dissipative code, Enzo, around $k = 40$. The power law form of the power spectrum may therefore be deceiving (as evidence of numerical convergence), because it's slope is apparently dependent on the numerical diffusivity. It is only by comparing different codes or the same code with different values of the diffusivities that we can find a truly converged power spectrum. If the power spectrum is not converged to its correct slope, due to a lack of dynamic range of scales or an excess of numerical diffusivity, the slope of the mass distribution may be strongly affected. For example, in the MHD case we get $x = 1.4$ from the Stagger code, and $x = 1.7$ from the Zeus code. It is possible that even the Stagger code power spectrum is not fully converged, and that the correct value is approximately $\beta = 1.8$, in which case the slope is $x = 1.36$. This is suggested by the fact that in the HD regime PPM has a slightly smaller exponent than in the HD regime of the Stagger code. Padoan et al. (2006) have recently obtained an accurate measurement of the velocity power spectrum in the Perseus molecular cloud complex. Their result is $\beta = 1.81 \pm 0.10$, accurate enough to rule out the significantly larger power spectrum slopes produced by more dissipative SPH simulations (see § 4).

3. MASS DISTRIBUTIONS

We compute the mass distribution of gravitationally unstable cores formed in turbulence simulations without self-gravity primarily to learn about the effect of turbulence under different conditions, for example with and without magnetic fields, and to compare with the predictions of the turbulent fragmentation model. The question of how self-gravity would modify the mass distribution is a separate one, and will not be addressed in this work. However, it is important to stress that the present result are obtained after the driven turbulence has been statistically relaxed, which could not be achieved with self-gravity. The mass distributions derived in this work and the mass distribution predicted by Padoan & Nordlund (2002), can therefore represent,

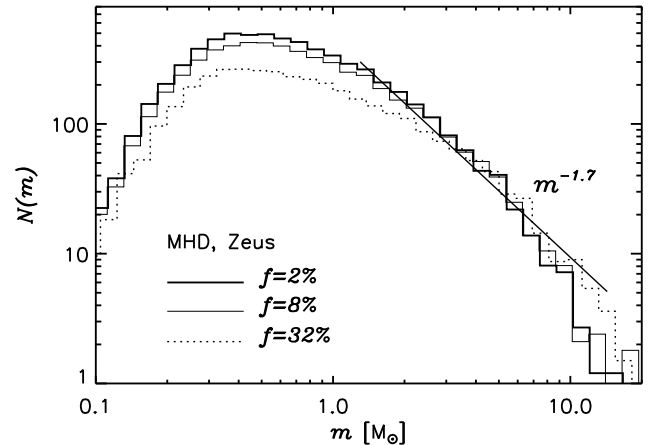


FIG. 8.— Same as Figure 7, but from the Zeus MHD run.

at best, a guess of the final outcome of more realistic simulations with self-gravity. In such simulations including self-gravity the mass distribution of unstable cores may initially vary with time, as the most massive cores are still being assembled by converging turbulent flows while their central part has already collapsed.

Cores are defined as connected overdensities that cannot be split into two or more overdensities of amplitude $\delta\rho/\rho > f$. The unstable cores are simply the cores with mass larger than their Bonnor-Ebert mass. These definitions are implemented in our clumpfind algorithm by scanning the density field with discrete density levels, each of amplitude f relative to the previous one. Only the connected regions above each density level that are larger than their Bonnor-Ebert mass are selected as unstable cores. After this selection, the unstable cores from all levels form a hierarchy tree. Only the final (unsplit) core of each branch is retained. It is important to impose the Bonnor-Ebert condition while building the tree, otherwise some large unstable cores would be incorrectly eliminated if they split into smaller cores that were later rejected based on the Bonnor-Ebert condition.

Clumpfind algorithms differ in the way they assign the surrounding mass to the cores. The popular algorithm by Williams, de Geus, & Blitz (1994), for example, uses up all the available mass (see their Figure 2). This results in a core formation efficiency of 100% above the threshold density, which is an artifact of that algorithm with no physical justification, though it may mimic a process of competitive accretion. Our algorithm, instead, assigns to each core only the mass within the density isosurface that defines the core (below that density level the core would be merged with its next neighbor). We prefer this definition because the smallest possible mass is assigned to each core and we want to study the effect of turbulent fragmentation in isolation, not trying to guess the outcome of the subsequent accretion. It turns out that, with this definition, and under conditions typical of molecular clouds, the unstable cores contain a few percent of the total mass. This suggests that not much of the remaining mass will ever be accreted, as we know that the star formation efficiency in molecular clouds is approximately a few percent.

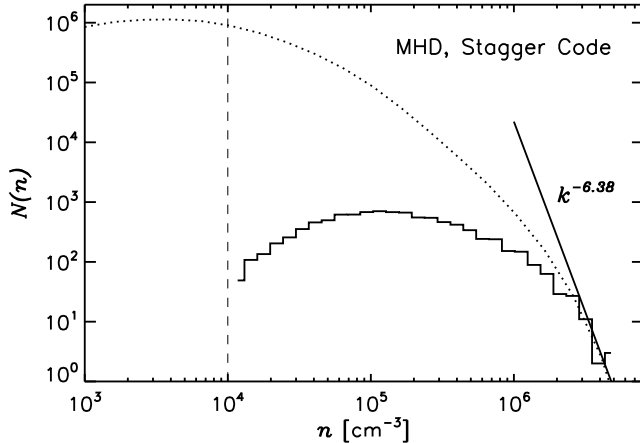


FIG. 9.— Mean density distributions of the unstable cores selected from two snapshots of the Stagger Code MHD experiment (solid histogram), assuming a mean gas density of 10^4 cm^{-3} and a 6 pc size, as in previous figures. The dotted curve is the pdf of gas density of the whole computational domain, computed for the same two snapshots. The solid straight line shows the power law distribution of core mean densities that would be derived from the velocity scaling, $N(n) \propto n^{-6/(\beta-1)}$, using the specific value of $\beta = 1.94$ found in those two snapshots. The vertical dashed line marks the mean gas density. The two curves and the power law are normalized to approximately match each other at the largest densities, to illustrate that a very large fraction of the densest gas is found within unstable cores, while gas of decreasing density is increasingly harder to capture in unstable regions.

Once the physical size and mean density of the system are chosen, the clumpfind algorithm depends only on two parameters: i) The spacing of the discrete density levels, f , and ii) the minimum density above which cores are selected, ρ_{\min} . In principle there is no need to define a minimum density, but in practice it speeds up the algorithm. We have verified that results (including the total mass in cores) do not change significantly for values of ρ_{\min} below the mean gas density, so we scan the density field only above the mean density. Notice that only half of the volume, but most of the mass, is found above the mean density, because, according to the lognormal pdf, most of the mass is packed in a small volume fraction.

The parameter f may be chosen according to a physical model providing the value of the smallest density fluctuation that could collapse separately from its contracting background. However, given the difficulty of predicting the outcome of the gravitational fragmentation, we prefer to simply search for a convergence of the mass distribution with decreasing values of f . Luckily, the convergence is typically obtained already at a value of $f \approx 16\%$, meaning that differences between the mass distributions with $f = 8\%$ and 16% are generally insignificant. The cores are therefore well defined, and in most cases they correspond to density fluctuations, relative to the surrounding gas, even much larger than f .

In Figure 4 the mass distributions above $1 M_{\odot}$ are plotted for the main four experiments scaled to a mean density of 10^4 cm^{-3} , a box size of 6 pc, and a clumpfind density resolution $f = 8\%$. Overplotted on the corresponding power law section of each mass distribution, the dashed lines show the power law derived from the power spectrum slope and the shock jump conditions of each simulation, according to the turbulent fragmenta-

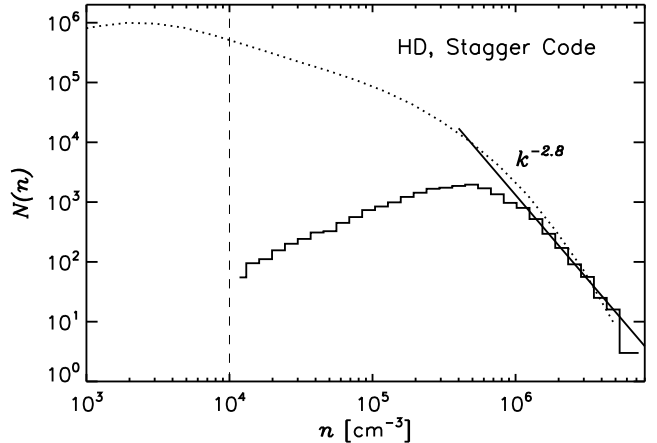


FIG. 10.— Same as Figure 9, but for one snapshot of the Stagger Code HD run. The power law here is $N(n) \propto n^{-3/(\beta-1)}$, with the value of $\beta = 2.06$ computed for this snapshot.

tion model, $x = 3/(4 - \beta)$ in the MHD regime, and $x = 3/(5 - 2\beta)$ in the HD regime. The general trend is recovered well, despite deviations to be expected because this mass distributions are from single snapshots, not time averages.

Figure 5 shows the mass distributions of the HD and MHD regimes (Enzo and Stagger Code respectively), computed with $f = 16\%$ and assuming a mean gas density of 10^4 cm^{-3} . Each mass distribution is the result of matching two mass distributions, computed for a computational box size of 1 pc and 6 pc. The 6 pc case makes it possible to sample masses in the range $1 - 10 M_{\odot}$, and hence to probe the effect of the turbulence power spectrum and shock jump conditions on the mass distribution, but suffers from incompleteness for stars below $1 M_{\odot}$. The 1 pc case samples well the turnover region, and hence defines the peak mass for that mean density and rms Mach number, but does not yield intermediate and high mass stars. Figure 6 is equivalent to Figure 5, but uses the MHD Zeus run, instead of the Stagger Code run.

The numerical mass distributions reproduce the sharp difference between the HD and MHD regimes predicted by the turbulent fragmentation model. The steeper mass distribution expected from the Zeus run, compared with the Stagger Code run, due to the steeper Zeus turbulence power spectrum, is also recovered. The slopes predicted by the turbulent fragmentation model are overplotted in each figure. Furthermore, the MHD regime yields a mass distribution of gravitationally unstable cores practically indistinguishable from Chabrier's stellar IMF (Chabrier 2003), both in the Zeus and in the Stagger Code runs. Finally, the Stagger Code HD run also yields a mass distribution consistent with the model prediction (see for example Figure 4). The relation between the mass distribution and the power spectrum and shock jump conditions is therefore successfully tested with 3 different codes at very high numerical resolution. As discussed below, the model predictions for the HD regime are also qualitatively confirmed with a fourth code (the TVD code), at lower resolution.

To verify the convergence of the clumpfind algorithm

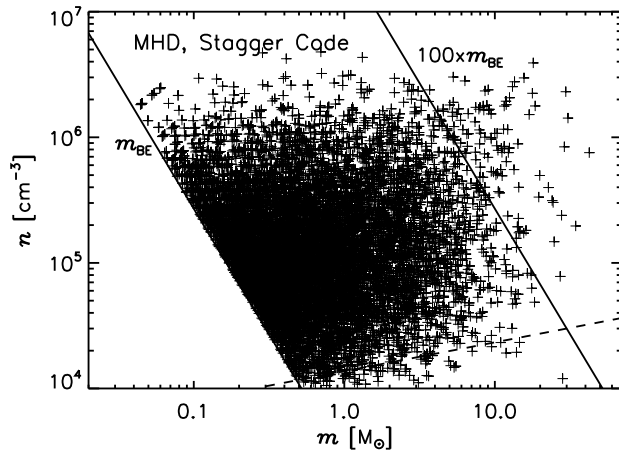


FIG. 11.— Mean density versus mass, of the unstable cores selected from two snapshots of the Stagger Code MHD run, assuming a mean gas density of 10^4 cm^{-3} and a 6 pc size, as in previous figures. The solid line on the left marks the Bonnor-Ebert mass, while the solid line on the right a mass 100 times larger than the Bonnor-Ebert value. The turbulence produces a range of masses and mean densities of unstable cores spanning three orders of magnitude. The dashed line is the power law relation between mean density and mass based on the average scale dependence of these two quantities, $n \propto m^{(\beta-1)/(8-2\beta)}$, using $\beta = 1.94$, as in Figure 9.

with respect to the density resolution, expressed by the parameter f , we plot in Figures 7 and 8 the mass distributions of the MHD regime assuming a mean gas density of 10^4 cm^{-3} and a 6 pc size. Figure 7 is from the Stagger Code MHD run and Figure 8 from the Zeus MHD run. For this convergence study we have computed together the mass distributions of unstable cores selected from three different snapshots. With these larger samples, statistical deviations are reduced, resulting in a more sensitive test of convergence. Between $f = 32\%$ and $f = 8\%$ there is a tendency to fragment the largest cores and create a larger number of small cores. However, the differences between $f = 8\%$ and $f = 2\%$ are rather small. Furthermore, the slope of the mass distribution above $2\text{--}3 M_\odot$ is rather independent of resolution, even if the power law section of the mass distribution tend to move slightly to larger masses at very large values of f .

4. DISCUSSION

4.1. Variance Versus Scaling

The turbulent fragmentation model estimates the mass distribution of unstable cores, based on the assumption that their size is determined by the thickness of post-shock layers. So far we have used the simulations and the clumpfind algorithm to confirm the predicted relation between the slope of the mass distribution and that of the velocity power spectrum. The model also implies that, on the average, the *size* and *mean density* of cores should be scale dependent as well, at least for cores significantly more massive than the average Bonnor-Ebert mass. In the absence of variance, the distributions of core properties are derived from their scale dependence assuming the self-similar distribution of scales, $N(L) \propto L^{-3}$. A quantity X , scaling like $X \propto L^a$, would have a power law distribution $N(X) \propto X^{-3/a}$, where the distributions are expressed as probability densities per logarithmic intervals (or, equivalently, they can be thought of as cumula-

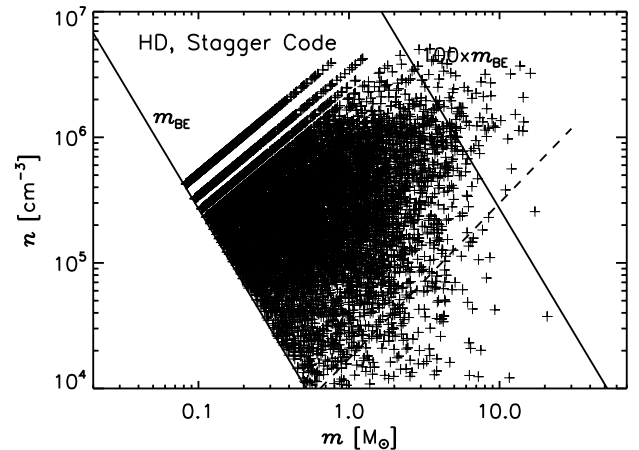


FIG. 12.— Same as Figure 11, but for the cores selected from one snapshot of the Stagger Code HD run. The dashed power law here is $n \propto m^{(\beta-1)/(5-2\beta)}$, with the value of $\beta = 2.06$ computed for this snapshot.

tive functions derived from the integration of probability densities per linear intervals). A very steep distribution of a quantity X is therefore equivalent to a weak scale dependence of X (small values of the exponent a), resulting in a limited range of values of X caused by its scale dependence alone.

However, the properties of cores arising in turbulent supersonic flows are random variables following some distributions that can be roughly characterized by their standard deviation. This must be true on any scale. If the standard deviation of the distribution at a fixed scale is very large, it may exceed the range of values expected from the scale dependence, and the full distribution (integrated over all scales) may resemble more the distribution at a fixed scale than the power law predicted from the scale dependence. In the case of the core mass distributions in both the MHD and HD regimes, $a > 1$, meaning that the logarithmic range of core masses exceeds the logarithmic range of scales, and therefore the scale dependence is expected to leave a strong imprint in the mass distributions. This is a case in which the scale dependence of a quantity results in a well defined power law distribution of that quantity. If instead the scale dependence of a quantity X is weak ($a < 1$), it may be completely masked by the variance of its distribution at a fixed scale.

Let's consider first the distribution of the core mean density. According to our model, the scaling of velocity results in the core mean density distribution $N(n) \propto n^{-6/(\beta-1)} = n^{-6.67}$, in the MHD regime, and $N(n) \propto n^{-3/(\beta-1)} = n^{-3.33}$ in the HD regime, where the numerical estimate of the exponents assumes $\beta = 1.9$. These density distributions are both steeper than the corresponding mass distributions, while the effect of the variance in density should be comparable to that in mass, as mass is proportional to density. Therefore, even if the mass distributions have power law tails, the core mean density distributions may not show any power law. This is certainly the case in the MHD regime, given the very large exponent and hence the very weak scale dependence of the mean density (very narrow range of densities over

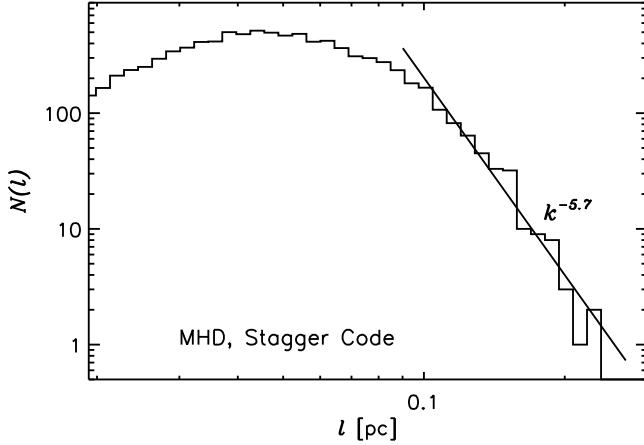


FIG. 13.— Size distribution of the unstable cores selected from the same two snapshots of the Stagger Code MHD experiment as in the left panels of Figures 9 and 11. The core size is defined as the cubic root of its volume. The power law distribution resulting from the scale dependence of the core size, $N(l) \propto l^{-6/(3-\beta)}$, is plotted as a solid line, using the value of $\beta = 1.94$ found in the two snapshots.

a large range of scales).

In Figures 9 and 10 we show the MHD and HD mean density distributions of unstable cores from the Stagger Code experiments (solid histograms), the power laws based on the velocity scaling (straight solid lines) and the pdf of gas density from the whole computational volume (dotted curves). Consistent with the arguments above, in the MHD regime there is no evidence of the power law scaling, while in the HD regime a short power law is visible, with a slope consistent with the model prediction. Notice how the core mean density distribution gradually departs from the general density pdf toward lower densities, as a result of the selection of only gravitationally unstable cores. This large amount of gas mass not locked in unstable cores, even at relatively high densities, illustrates how the turbulence controls the efficiency of the star formation process.

The weak scale dependence of the core mean density can also be appreciated by plotting the core mean density versus the core mass, as done in Figures 11 and 12. These scatter plots don't show much evidence of the power law relation of mean density and mass from the scale dependence of these two quantities, $n \propto m^{(\beta-1)/(8-2\beta)} = m^{0.21}$ in MHD, and $n \propto m^{(\beta-1)/(5-2\beta)} = m^{0.75}$ in HD, assuming again $\beta = 1.9$ in the numerical estimates. At any given mass, the density may span almost three orders of magnitude, although most values are within an factor of ten range. This large variance is unavoidable in isothermal supersonic turbulence, due to the broad Lognormal density pdf, with standard deviation approximately equal to half the rms Mach number of the turbulence.

The average value of the core size should also be scale dependent, with the corresponding distributions being $N(l) \propto l^{-6/(3-\beta)} = l^{-5.45}$ in MHD and $N(l) \propto l^{-3/(2-\beta)} = l^{-30}$ in HD (assuming $\beta = 1.9$ in the numerical estimates). The MHD power law is rather steep, but the density variance translates into a smaller size

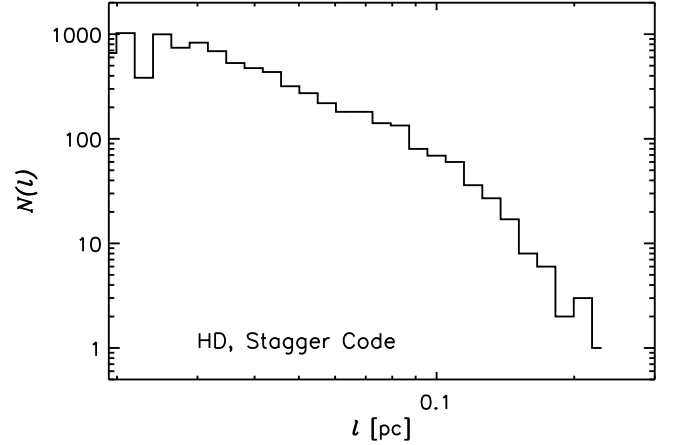


FIG. 14.— Same as in Figure 13, but for the Stagger Code HD experiment. The scaling law would now give an extremely steep power law, $N(l) \propto l^{-3/(2-\beta)}$, or essentially no size range.

variance, as $l \propto n^{-1/3}$, so even a rather weak scale dependence may result in a power law size distribution. In the HD regime, there is almost a perfect cancellation of the scale dependence of the shocked layer column density and volume density, making the average thickness of such a layer almost scale independent. The resulting power law distribution would be so steep, that even a small variance would completely mask it.

Figures 13 and 14 show the core size distribution of the same cores as in Figures 9 to 12. The core size is defined as the cubic root of its volume. The power law distribution of the mean core size resulting from the scale dependence is plotted as a solid line in the MHD case, with the exponent corresponding to a value of $\beta = 1.94$, as measured from the two snapshots used to select the cores. In the MHD experiment there is some evidence of a power law tail, with the same slope as inferred from the scale dependence of our model. In the HD regime, instead, there is no evidence of the power law tail, as that would correspond to a sharp cutoff, which is easily masked by the variance of the size distribution at a fixed scale.

In summary, based on the competition between variance and scaling in establishing statistical distributions of core properties, we expect to find power law tails in the distributions of masses and sizes in the MHD regime, and only masses (or marginally densities) in the HD regime. The unstable cores selected from our numerical experiments have clear power law tails only in the case where these are expected, and in such cases the power law slopes are those predicted by the model. In Padoan and Nordlund (2002) the competition between the variance and the scaling is responsible for the flattening and the turnover of the mass distribution toward smaller masses, because toward smaller masses the selection of the unstable cores becomes increasingly sensitive to their density. At large masses, because the scaling is the dominant effect, the variance is neglected.

In numerical simulations, even when the variance should not be dominant, power law tails may be absent from statistical distributions of core properties, as a result of the limited range of scales relative to the actual

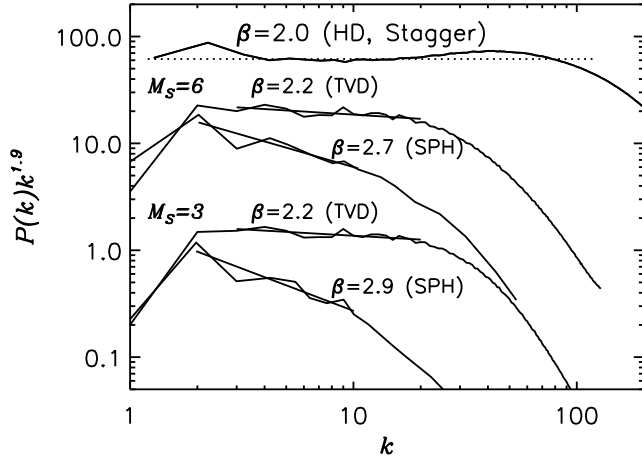


FIG. 15.— Power spectra compensated for the slope of the Stagger-Code HD run, $\beta = 1.9$. The TVD and SPH power spectra are the same as in Figure 2 of Ballesteros-Paredes et al. (2006), for the Mach numbers 3 and 6.

interstellar turbulence. If the range of scales is reduced, the range of values in core properties due to the scale dependence is also reduced, possibly to the point of becoming smaller than the variance of the distribution at a fixed scale. Lognormal-like tails may then cut short the power law distributions, as a numerical effect.

It is important to appreciate that a driven turbulent flow may experience, over time, significant deviations from its average scaling laws, and that this may be the explanation for observed variations of the stellar IMF from place to place much in excess of the Poisson variance related to the statistical sample size. The scaling laws were understood phenomenologically by Kolmogorov as due to a scale independent energy dissipation rate, arising from an efficient energy cascade from large to small scales in turbulent flows. This transfer from large to small scales takes approximately a dynamical time of the outer scale. Therefore, in a driven flow, any variations of the energy injection rate on a time-scale of order the dynamical time causes a “bump” in inertial-range scaling laws that has to propagate down the turbulent cascade, until it reaches the small viscous scales after approximately a dynamical time of the outer scale. Because the typical lifetime of star-forming regions is comparable to this dynamical time (and star formation starts immediately when a molecular cloud is assembled), the turbulence can hardly be considered relaxed, and large variations of the IMF from place to place should be expected. These variations should not be interpreted as the lack of a universal process of star formation, but rather as the evidence of both its turbulent origin and its short lifetime.

4.2. Previous Results

Ballesteros-Paredes et al. (2006) argue that the fragmentation model of Padoan and Nordlund (2002) is in contradiction with their numerical results, based on TVD and SPH simulations without magnetic fields. They conclude that the core mass distribution depends on the rms Mach number, but fail to point out that the Padoan and Nordlund model contains such a Mach number dependence, with the peak of the mass distribution shifting

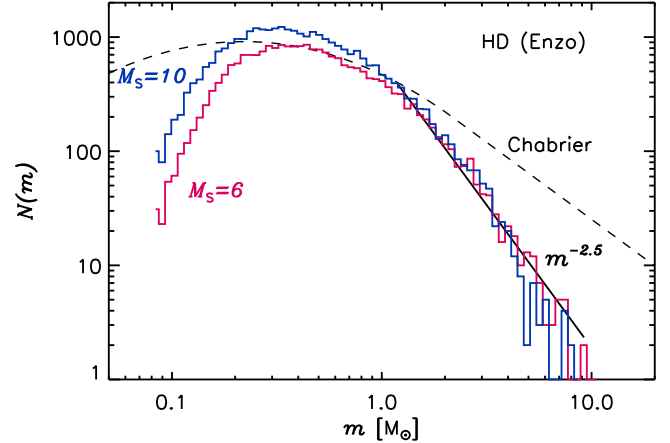


FIG. 16.— Mass distributions of gravitationally unstable cores from the Enzo HD runs with $M_S = 6$ and $M_S = 10$, $f = 8\%$ and assuming a mean gas density of 10^4 cm^{-3} and a box size of 6 pc. Each mass distribution contains unstable cores from two snapshots. The Chabrier (2003) IMF (dashed line) and the power law predicted by the turbulent fragmentation model (solid line) are also plotted.

to lower masses as the Mach number increases, in agreement with the numerical results in Ballesteros-Paredes et al. (2006). In the Padoan and Nordlund model, the slope of the mass distribution for masses above the peak is independent of the Mach number, also in agreement with the results of Ballesteros-Paredes et al. (2002) based on the TVD simulations (see their Figure 4), but in contradiction with their SPH simulations (see their Figure 5).

Figure 15 compares the power spectrum from the Stagger-Code HD run with two TVD and two SPH power spectra from Ballesteros-Paredes et al. (2006), for Mach numbers 3 and 6. The inertial range in both the TVD and SPH cases is not very extended, due to the low numerical resolution. The TVD code gives a slope of $\beta \approx 2.2$, the same value found in the Zeus run, for both Mach numbers. The extent of the inertial range in the TVD run is also comparable to the Zeus result at the same resolution (not shown). The power spectra of the SPH runs are instead much steeper, and their slope increases with decreasing Mach number, $\beta \approx 2.7$ for $M_S \approx 6$ and $\beta \approx 2.9$ for $M_S \approx 3$. As shown by the TVD runs, the power spectrum should not vary much with Mach number between $M_S = 6$ and $M_S = 3$. For lower Mach numbers, the power spectrum should become shallower, and converge to a value of $\beta \approx 5/3$ for $M_S < 1$. The SPH power spectrum slope is therefore much too steep and its Mach number dependence unphysical.

In summary, it appears that the TVD runs of Ballesteros-Paredes et al. (2006) are able to qualitatively reproduce the turbulent fragmentation process that we have tested in the present work with much larger numerical resolution, with three different grid-based codes and both with and without magnetic fields. The complete absence of an inertial range with a reasonable slope, or with a reasonable dependence of the slope on the Mach number, makes their SPH simulations totally inadequate for testing the turbulent fragmentation model, as the model relies on the scale-free nature of turbulent flows. Nevertheless, Ballesteros-Paredes et al. (2006) seem to base

their conclusions partly on the SPH results, even if in contradiction with their own more robust TVD results that are confirmed here.

Ballesteros-Paredes et al. (2006) try to argue that the magnetic field plays no role in the IMF, to justify the relevance of their simulations without magnetic fields. However, we have shown here that the HD regime produces much steeper mass distributions than the MHD regime. The HD regime is therefore a poor choice of physical parameters, if the aim is to extract the power law mass distribution from simulations with a very limited numerical resolution, as it is much more variance-dominated than the MHD regime. As explained above, it is not surprising that the very limited tails of their power laws may possibly appear more Lognormal than straight.

To address directly the issue of the Mach number dependence of the mass distribution, raised by Ballesteros-Paredes et al. (2006), we plot in Figure 16 the mass distributions from the Enzo HD runs with $M_S = 6$ and $M_S = 10$ and with $f = 8\%$. These mass distributions are computed assuming a mean gas density of 10^4 cm^{-3} and a box size of 6 pc. Each distribution contains cores from two snapshots. The Figure shows that the power law part of the mass distribution, above $1\text{--}2 M_\odot$, is independent of the Mach number and matches the prediction of the turbulent fragmentation model, that is $k^{-2.5}$ for the power spectrum slope $\beta = 1.9$ of the HD Enzo runs.

5. CONCLUSIONS

We have used large numerical simulations of supersonic MHD and HD turbulence to test the turbulent fragmentation model of Padoan and Nordlund (2002). The model predicts a power law distribution for large masses, related to the turbulence energy power spectrum slope, and the shock jump conditions. This power law mass distribution is confirmed by the numerical experiments. The model also predicts that the HD regime should yield a much steeper mass distribution of unstable cores than the MHD regime, which is confirmed by the simulations. This feature of the fragmentation model is very important because it shows that even rather weak magnetic fields (super-Alfvénic turbulence) can be crucial in setting the initial conditions for the process of star formation and in shaping the stellar IMF.

While present-day star formation takes place probably always in the MHD regime, star formation at very high

redshift may well occur in the HD regime, both because the field strength is still low and because the value of the critical magnetic field strength that defines the HD regime is larger at higher temperatures. The IMF of the earliest population II stars, and perhaps the latest population III stars as well, may be formed in turbulent environments in this HD regime, resulting in an IMF narrowly peaked around a mass of order $10 M_\odot$. The effect of such a peculiar IMF of early stellar populations on the ionization history and metallicity evolution of the universe should be investigated.

Numerical simulations can quantitatively account for the fundamental role of the turbulence in setting the initial conditions for the process of star formation only if they can generate an inertial range of turbulence, which requires both low numerical diffusivity and large numerical resolution. Furthermore, to model present-day star formation that occurs in the MHD regime, the magnetic field cannot be neglected, *even if the turbulence is assumed to be super-Alfvénic*. SPH simulations of large scale star formation to date fail in all three fronts: numerical diffusivity, numerical resolution and presence of magnetic fields. This should cast serious doubts on the value of comparing predictions based on SPH simulations with observational data (see also Agertz et al. 2006).

Finally, the mass distribution of unstable cores found in the MHD simulations is indistinguishable from the Chabrier stellar IMF (Chabrier 2003) and in qualitative agreement with the less well determined mass distributions of prestellar cores selected from dust emission or molecular line observations. Such a coincidence may indicate that gravitational fragmentation, competitive accretion or merging, all absent in these turbulence simulations, may not play a major role in the origin of the stellar IMF, a fascinating idea to be tested with the next generation of high resolution simulations of self-gravitating turbulence.

This research was partially supported by a NASA ATP grant NNG056601G, by an NSF grant AST-0507768, and by a NRAC allocation MCA098020S. We utilized computing resources provided by the San Diego Supercomputer Center, by the National Center for Supercomputing Applications and by NASA High End Computing Program.

REFERENCES

- Abel, T., Bryan, G. L., & Norman, M. L. 2000, ApJ, 540, 39
 Agertz, O. et al. 2006, astro-ph/0610051
 Ballesteros-Paredes, J., Gazol, A., Kim, J., Klessen, R. S., Jappsen, A.-K., & Tejero, E. 2006, ApJ, 637, 384
 Basu, S. 2000, ApJ, 540, L103
 Beck, R. 2001, Space Science Reviews, 99, 243
 Beuther, H., Zhang, Q., Sridharan, T. K., Lee, C.-F., & Zapata, L. A. 2006, A&A, 454, 221
 Bourke, T. L., Myers, P. C., Robinson, G., & Hyland, A. R. 2001, ApJ, 554, 916
 Chabrier, G. 2003, PASP, 115, 763
 Crutcher, R. M. 1999, ApJ, 520, 706
 Dobler, W., Haugen, N. E., Yousef, T. A., & Brandenburg, A. 2003, Phys. Rev. E, 68, 026304
 Falkovich, G. 1994, Physics of Fluids, 6, 1411
 Han, J. L., Ferrière, K., & Manchester, R. N. 2004, ApJ, 610, 820
 Haugen, N. E., & Brandenburg, A. 2004, Phys. Rev. E, 70, 026405
 Iliev, I. T., Mellema, G., Shapiro, P. R., & Pen, U.-L. 2006, astro-ph/0607517
 Jimenez, R., & Haiman, Z. 2006, Nature, 440, 501
 Luhman, K. L. 2004, ApJ, 617, 1216
 Myers, P. C., & Goodman, A. A. 1988, ApJ, 326, L27
 Norman, M. L., & Bryan, G. L. 1999, ASSL Vol. 240: Numerical Astrophysics, 19
 Ossenkopf, V., Trojan, C., & Stutzki, J. 2001, A&A, 378, 608
 Padoan, P., & Nordlund, Å. 1999, ApJ, 526, 279
 Padoan, P., & Nordlund, Å. 2002, ApJ, 576, 870
 Padoan, P., Juvela, M., Kritsuk, A., & Norman, M. L. 2006, ApJ, in press
 Palla, F., Salpeter, E. E., & Stahler, S. W. 1983, ApJ, 271, 632
 Salpeter, E. E. 1955, ApJ, 121, 161
 Stone, J. M., & Norman, M. L. 1992, ApJS, 80, 791
 Williams, J. P., de Geus, E. J., & Blitz, L. 1994, ApJ, 428, 693